Regulatory T cells promote myelin regeneration in the central nervous system

Dombrowski, Y., O'Hagan, T., Dittmer, M., Penalva, R., Mayoral, S. R., Bankhead, P., ... Fitzgerald, D. C. (2017). Regulatory T cells promote myelin regeneration in the central nervous system. Nature Neuroscience, 20(5), 674–680. DOI: 10.1038/nn.4528

Published in:
Nature Neuroscience

Document Version:
Peer reviewed version

Queen's University Belfast - Research Portal:
Link to publication record in Queen's University Belfast Research Portal

Regulatory T cells promote myelin regeneration in the Central Nervous System

Yvonne Dombrowski[1], Thomas O'Hagan[1], Marie Dittmer[1], Rosana Penalva[1], Sonia R. Mayoral[4], Peter Bankhead[2], Samara Fleville[1], George Eleftheriadis[1], Chao Zhao[3], Michelle Naughton[1], Rachel Hassan[1], Jill Moffat[1], John Falconer[1], Amanda Boyd[8], Peter Hamilton[2], Ingrid V. Allen[1], Adrien Kissenpfennig[1], Paul N. Moynagh[1,5], Emma Evergren[2], Bernard Perbal[6,7], Anna C. Williams[8], Rebecca J. Ingram[1], Jonah R. Chan[4], Robin J.M. Franklin[3] and Denise C. Fitzgerald[1,*]

[1]Centre for Experimental Medicine, School of Medicine, Dentistry and Biomedical Science, Queen's University Belfast, Northern Ireland, UK

[2]Centre for Cancer Research and Cell Biology, School of Medicine, Dentistry and Biomedical Science, Queen's University Belfast, Northern Ireland, UK

[3]Wellcome Trust-Medical Research Council Cambridge Stem Cell Institute, Clifford Allbutt Building, Cambridge Biomedical Campus, University of Cambridge, UK

[4]Department of Neurology and Program in Neurosciences, University of California, San Francisco, USA

[5]Institute of Immunology, Department of Biology, National University of Ireland Maynooth, Ireland.

[6]Université Paris 7- D. Diderot, Paris, France

[7]Université Côte d'Azur, CNRS, GREDEG, France and International CCN Society

[8]Centre for Regenerative Medicine, University of Edinburgh, Edinburgh, UK

*Corresponding author: d.fitzgerald@qub.ac.uk

Abstract

Regeneration of central nervous system (CNS) myelin involves differentiation of oligodendrocytes from oligodendrocyte progenitor cells (OPC). In multiple sclerosis (MS), remyelination can fail despite abundant OPC, suggesting impairment of oligodendrocyte differentiation. T cells infiltrate the CNS during MS, yet little is known about T cell functions in remyelination. Here, we report that regulatory T cells (T_{reg}) promote oligodendrocyte differentiation and (re)myelination. T_{reg}-deficient mice exhibited significantly impaired remyelination and oligodendrocyte differentiation that was rescued by adoptive transfer of T_{reg}. In brain slice cultures, T_{reg} accelerated developmental myelination and remyelination, even in the absence of overt inflammation. T_{reg} directly promoted OPC differentiation and myelination *in vitro*. We identified CCN3 as a novel T_{reg}-derived mediator of oligodendrocyte differentiation and myelination *in vitro*. These findings reveal a new regenerative function of T_{reg} in the CNS, distinct from immunomodulation. Although originally named 'T_{reg}' to reflect immunoregulatory roles, this also captures emerging, regenerative T_{reg} functions aptly.

Introduction

The failure to reinvest demyelinated axons with new myelin sheaths results in a lack of axonal conduction and metabolic support. This ultimately leads to irreversible axonal loss that typifies later stages of chronic demyelinating diseases such as MS, leaving patients with permanent neurological disability[1,2]. Remyelination frequently occurs in the context of innate and adaptive immune responses[3,4]. T cells can act as effectors of myelin damage but are also required for successful remyelination[5]. However, T cells encompass a range of phenotypically and functionally distinct subsets and contributions of T cell subsets to CNS remyelination are poorly understood. Since inflammation-resolving effects of T_{reg} frequently coincide with tissue regeneration, we hypothesized that T_{reg} promote remyelination.

Results

T_{reg} are required for efficient OPC differentiation during remyelination *in vivo.*

To study regenerative T cell functions in remyelination *in vivo*, distinct from classical T cell-mediated demyelination observed in experimental autoimmune encephalomyelitis (EAE), focal demyelination was induced by injecting lysolecithin into spinal cord white matter of mice. Such lesions naturally remyelinate within one month and follow a well-defined time-course with distinct phases of OPC activation, recruitment and oligodendrocyte differentiation[6,7]. Flow cytometric immunophenotyping at 3 days post lesion (d.p.l.) demonstrated an abundance of $CD45^+CD11b^+$ myeloid cells in lesioned tissue as previously described[8]. However, distinct, albeit smaller populations of $CD3^+$ and $CD4^+$ T cells were also evident even up to 11 d.p.l., including $CD3^+CD4^+Foxp3^+$ T_{reg}, a T cell population recently implicated in tissue regeneration[9,10] (Supplementary Fig. 1a-e). To determine if T_{reg} were functionally important in remyelination, we used Foxp3-DTR transgenic mice in which diphtheria toxin (DT) administration depletes Foxp3-expressing cells[11] (Supplementary Fig. 1f). Chronic DT exposure causes toxicity and considerable morbidity even in wild-type mice[12-14] while T_{reg} deficiency induces systemic immune activation[11], precluding long-term studies. Therefore, densities of $CC1^+Olig2^+$ differentiated oligodendrocytes, as an established surrogate readout of remyelination[15], were compared at 14 d.p.l. and electron microscopy was performed at 17 d.p.l.

T_{reg}-depleted animals exhibited significantly fewer differentiated $CC1^+Olig2^+$ oligodendrocytes than non-depleted animals or DT-treated wild-type controls (Fig. 1a,b). Mice lacking T_{reg} exhibited comparable lesion sizes (Fig. 1c) indicating that T_{reg} are not required to limit tissue damage in this model and crucially, that experimental groups had comparable burdens of demyelination to repair. Reduced numbers of $CC1^+Olig2^+$ cells in T_{reg}-depleted mice could have arisen because of a failure to recruit sufficient OPC to the demyelinated area. However, no significant differences in $Olig2^+Ki67^+$ proliferating OPC at 5 d.p.l. or 10 d.p.l. were observed between groups (Fig. 1d and Supplementary Fig. 1g) indicating that reduced generation of oligodendrocytes was likely due to impairment in

differentiation. Restricting T_{reg} depletion only to the pre-lesioning phase did not alter $CC1^+Olig2^+$ cell numbers (Supplementary Fig. 1h), suggesting that T_{reg} are important in later stages of remyelination. Indeed electron microscopic analysis of lesions demonstrated significantly fewer remyelinated axons in T_{reg}-depleted animals (Fig. 1e). To further test the role of T_{reg} in remyelination using a gain-of-function model, MACS-purified wild-type T_{reg} were injected into T_{reg}-deficient animals ('injected T_{reg}'). T_{reg} administration significantly increased numbers of $CC1^+Olig2^+$ differentiated oligodendrocytes in lesions, demonstrating the capacity of T_{reg} to rescue impaired oligodendrocyte differentiation *in vivo* (Fig. 1f,g). To verify the importance of T_{reg} in myelin regeneration in a second remyelinating model as well as at a different CNS site, demyelination was induced using cuprizone. Similar to results obtained using the spinal cord lysolecithin model, T_{reg} depletion significantly impaired $CC1^+Olig2^+$ oligodendrocyte differentiation in the corpus callosum of cuprizone-treated mice at day 14 of the remyelination phase (Fig. 1h,i) but not at day 10 (Supplementary 1i). This finding was supported by reduced PLP mRNA expression in T_{reg}-depleted animals at day 14 (Supplementary Fig. 1j). T_{reg} depletion did not significantly affect overall oligodendrocyte lineage numbers (Supplementary Fig. 1k) emphasizing the predominant effect of T_{reg} depletion on the differentiation phase of the regenerative response. These studies identify a novel role for T_{reg} in the process of oligodendrocyte differentiation and CNS remyelination in both brain and spinal cord *in vivo*.

T_{reg} directly promote brain tissue myelination and remyelination *ex vivo.*

Next, we asked if T_{reg} exerted direct regenerative effects within CNS tissue distinct from immunomodulation of infiltrating immune cells. To this end, we used neonatal murine organotypic brain slice cultures which naturally generate compact myelin *ex vivo* via OPC proliferation, differentiation and axonal ensheathment[16-19]. To determine if T_{reg} influence myelination, FACS-purified $CD4^+Foxp3\text{-}eGFP^+$ natural T_{reg} or control $CD4^+Foxp3^-$ conventional T cells (Tconv) were added directly onto slices. T cells infiltrated tissues and GFP^+ T_{reg} were still detectable within slices after 3 days *in vitro* (d.i.v.) (Supplementary Fig. 2a). Slices co-cultured with T_{reg} cells contained significantly

more MBP^+ oligodendrocytes and had significantly higher myelination index (myelin and axonal overlap, representing axonal ensheathment by myelin) at 3 d.i.v. than control slices without cells (Supplementary Fig. 2b-d) or slices with Tconv cells (Supplementary Fig. 2e). These findings demonstrate a myelinating action induced specifically by T_{reg}, rather than by activated T cells in general.

To investigate mechanisms of T_{reg}-induced myelination beyond cell-cell contact, slices were supplemented with conditioned media from $CD4^+$ T cells that were either polarized to a T_{reg} phenotype or were non-polarized (NP) to serve as activated T cell controls (Supplementary Fig. 2f), or control medium (control). T_{reg}-conditioned media significantly increased MBP^+ mature oligodendrocytes and myelination compared to controls at 7 d.i.v. (Fig. 2a-c, Supplementary Fig. 2g). These findings indicated that secreted factors drive oligodendrocyte differentiation and pro-myelinating effects of T_{reg}.

To test if T_{reg} also promoted regeneration of myelin, slices myelinated in culture for 14 days and were then demyelinated with lysolecithin for 16h. Addition of T_{reg}-conditioned media for 7 days following demyelination significantly increased MBP^+ mature oligodendrocytes (Fig. 2d,f) and myelination index (Fig. 2e,f Supplementary videos) compared to controls. These increases represented an acceleration of remyelination by T_{reg} as control slices eventually remyelinated after 2 weeks (Fitzgerald lab, data not shown). This was confirmed by electron microscopy showing significantly increased numbers of remyelinated axons in T_{reg}-treated slices compared to control, remyelinating slices (Supplementary Fig. 2h-j).

Although brain slices lack peripheral immune cells, CNS-resident microglia and astrocytes can generate local inflammatory responses upon slicing and demyelination[20,21] and therefore, effects of T_{reg} on (re)myelination could be due to known anti-inflammatory functions. Thus, to categorically test if T_{reg} directly promoted CNS myelination rather than indirectly via immunoregulation, slices were equilibrated for one week after slicing to allow pro-inflammatory cytokine production to subside[20] (Supplementary Fig. 2k) prior to addition of T cell-conditioned media for 7 days. In this model, slices

treated with T_{reg}-conditioned media again exhibited significantly higher MBP^+ oligodendrocyte numbers (Fig. 2g,i) and myelination index (Fig. 2h,i) than controls. These findings show that T_{reg} directly promote oligodendrocyte differentiation and myelin production under minimal-inflammatory conditions, suggesting a primary regenerative function of T_{reg} in the CNS distinct from, but complementary to, known immunomodulatory functions.

T_{reg} directly enhance oligodendrocyte differentiation and myelination *in vitro.*

To further investigate mechanisms of T_{reg}-induced remyelination via OPC differentiation, we next determined whether T_{reg} directly influenced glial cells using mixed glial cultures containing OPC as well as astrocytes and microglia (Supplementary Fig. 3a). Treatment with T_{reg}-conditioned media for 5 days significantly increased oligodendrocyte differentiation compared to control medium (Fig. 3a,b,d) and control non-polarized T cell-conditioned medium (Supplementary Fig. 3b,c), demonstrating direct T_{reg} signaling to glia. This effect was consistent independent of whether T_{reg} were induced from total $CD4^+$ T cells or from naïve $CD4^+$ T cells (Supplementary Fig. 3d). Supporting our *in vivo* findings, we observed no difference in oligodendrocyte lineage cell numbers (Fig. 3c), proliferation (Fig. 3e,f) or survival (Supplementary Fig. 3e,f).

As proof of principle that T_{reg} can directly modulate a regenerative cell population, independent of other CNS cells, pure OPC were cultured in the presence or absence of T cell-conditioned media. Within just two days, OPC treated with T_{reg}-conditioned media exhibited significantly more MBP^+ differentiated oligodendrocytes (Fig. 3g,h) demonstrating a direct action of T_{reg} on OPC. To test if this was functionally relevant, T_{reg}-conditioned media were added to OPC-dorsal root ganglion (DRG) neuron co-cultures. T_{reg} accelerated myelination of DRG neurons, evident within 4 days of stimulation with T_{reg}-conditioned media (Fig. 3i,j). Although not ruling out additional indirect mechanisms, these findings show that T_{reg}-secreted factors can directly signal to OPC to promote oligodendrocyte differentiation and functional myelination. This demonstrates for the first time that T_{reg} can alter the regenerative capacity of CNS progenitor cells.

CCN3 is produced by T_{reg} and promotes oligodendrocyte differentiation and myelination.

We next investigated T_{reg}-secreted factors that enhanced oligodendrocyte differentiation and myelination. Analysis of conditioned media by proteome profiling identified a number of candidate factors relevant to regeneration (Supplementary Fig. 4a), including CCN3 a growth regulatory protein with bioactivity in extracellular, cytoplasmic and nuclear compartments and implicated in regeneration of various tissues[22-25]. Dual ELISA and western blot validation confirmed that CCN3 was produced by T_{reg} (Fig. 4a,b). To determine if CCN3 mediated the oligodendrocyte-differentiating effect of T_{reg}, anti-CCN3 antibody was added to glial and brain slice cultures treated with T_{reg}-conditioned media for 5 and 7 days respectively. Anti-CCN3 antibody abolished T_{reg}-induced oligodendrocyte differentiation in glial cultures (Fig. 4c,d, Supplementary Fig. 4b) and inhibited the pro-myelinating effect of T_{reg} in brain slice cultures (Fig. 4e). To confirm these findings with a second loss-of-function approach, CCN3 was depleted from T_{reg}-conditioned media (Supplementary Fig. 4c, d) and recovered as eluted protein. T_{reg}-conditioned media depleted of CCN3 failed to promote oligodendrocyte differentiation in glial cultures (Fig. 4f) or brain slice myelination (Fig. 4g,h). Furthermore, treatment with recovered CCN3 significantly enhanced brain slice myelination (Fig. 4g,h). These studies implicate CCN3 as a novel T_{reg}-derived protein that mediates T_{reg}-driven OPC differentiation and CNS myelination.

Discussion

Immune-mediated tissue regeneration is an expanding field and recent studies highlight the importance of innate immune signaling in myelin regeneration[3,4,26]. Yet, despite decades of research into T cell-mediated pathogenesis and immunomodulation of CNS demyelination, very little is known about T cell functions in remyelination. Given that T cell-targeting therapies are used in MS, it is crucial to understand the full range of roles played by T cells. However, when interrogating immunoregenerative functions, appropriate choice of experimental models is crucial. T_{reg} limit damage in many inflammatory disease models including EAE. Overlapping tissue damage and

regeneration often occur in immune-mediated disease models such as EAE. Thus, true enhancement of regeneration can be challenging to distinguish from modulation of immunopathogenicity in these models. This motivated our choice of lysolecithin-induced demyelination in which the demyelinating insult is time-limited, clearly defined anatomically, independent of immune-driven tissue damage and follows a well-defined course of highly efficient myelin regeneration. With this approach, in combination with other models without peripheral immune influence such as OPC and brain slice cultures, we have uncovered a key regenerative function of T_{reg}. Mechanisms underlying this function include acceleration of oligodendrocyte differentiation and (re)myelination, via CCN3, a protein not previously known to target OPC, or indeed, to be produced by T_{reg}.

CCN3 is a growth regulatory protein with bioactivity in extracellular, cytoplasmic and nuclear compartments and is implicated in regeneration of various tissues[23-25,27,28]. CCN3 is expressed in the developing CNS[22,29] and glioma[30], but has not previously been implicated in CNS regeneration. Of note, we detected CCN3 expression in early organotypic brain slice cultures (Fitzgerald lab, data not shown) which may be developmentally regulated or due to tissue injury. In immune development, $CD34^+$ bone marrow progenitor cells express CCN3; however, ours is the first report that T_{reg}, or indeed any T cell population, produces CCN3. Together, these findings identify CCN3 as an immune effector molecule from early innate immune development to resolution of adaptive immune responses. This potentially places CCN3 at the leading edge of immune-mediated tissue regeneration and warrants investigation in immune cells at other anatomical sites. Interestingly, commercially sourced recombinant CCN3 did not induce oligodendrocyte differentiation (Fitzgerald lab, data not shown). This may be due to the lack of critical post-translational modifications in recombinant CCN3 and/or the presence of a 10-His tag at the C-terminus of the recombinant protein. This tag may impair bioactivity of this key functional region of CCN3, which contains a cysteine knot motif involved in homo- and heterodimerization. This emphasizes the importance of both gain-of-function and loss-of-function studies of CCN3 in reductionist and more complex models.

Recently Burzyn *et al.* identified roles for T_{reg} in muscle regeneration associated with local immunomodulation and amphiregulin expression[9] while Arpaia *et al*. reported TCR-independent tissue protective functions of amphiregulin-expressing T_{reg} in influenza-infected lungs[10]. Other studies described associations of T_{reg} with regeneration of cardiac muscle and neurons[31-33]. Here, we identified that T_{reg} directly promote oligodendrocyte differentiation and myelin production even in the absence of overt inflammation. Thus, signaling from T_{reg} can directly increase the regenerative capacity of a progenitor cell population, independent of immunomodulation known to support regeneration at other anatomical sites. This confers a primary regenerative role for T_{reg} complementary to, but distinct from, known immunomodulatory functions. In concert, these two functions confer fundamental damage-limiting and damage-resolving roles to T_{reg}. Therapies to boost tissue regeneration should consider this emerging and central role of T_{reg} in natural regeneration. This knowledge holds therapeutic potential for tissue regeneration in diseases such as MS.

Collectively, our novel findings and recent studies by others show that T_{reg} promote regeneration via different factors in different tissues. Our regenerative immunology study expands the classical functions of T-reg beyond reg-ulation to reg-eneration.

Acknowledgments

We thank A. Rudensky (Memorial Sloan Kettering Cancer Centre) for providing Foxp3-DTR mice and B. Malissen (Aix Marseille Université) for the provision of Foxp3-eGFP mice. We acknowledge extensive technical support from S. Leech, S. Peoples, N. de la Vega Gallardo, S. Mitchell, J. Brown, R. Blain and the staff of the animal facility. This work was supported by the Biotechnology and Biological Sciences Research Council (BB/J01026X/1, DF), The Leverhulme Trust (ECF-2014-390, YD), QUB (QUB - Lucy McGuigan Bequest, DF), The UK Multiple Sclerosis Society (941 and 50, RF and CZ), MRC UK Regenerative Medicine platform (MR/KO26666/1, AW), University of Edinburgh Wellcome Trust Multi User Equipment Grant (WT104915MA, AW), studentship support from Dept. for the Economy (Northern Ireland) and British Pathological Society, US National Multiple Sclerosis Society (RG5203A4, JC), NIH/NINDS (NS095889, JC), NIH/NIGMS IRACDA Postdoctoral Fellowship (K12GM081266, SM) and Wellcome Trust (110138/Z/15/Z, DF).

Author contributions

Experiments were designed, performed and analyzed by YD, TOH, MD, RP, SRM, SF, MN, GE, JM, JF, IVA, JRC and DCF. Image analysis tools were developed by PB and PH. EM was performed and analyzed by EE, AB and AW. CZ, RH, AK, PM, BP, RJI, JRC and RJMF provided advice on experimental design and interpretation, and IVA, PM and RJMF provided mentorship. Manuscript was written by YD and DCF with contributions from all authors. DCF oversaw the study.

Competing Financial Interest Statement

The authors have no competing interests as defined by Springer Nature, or other interests that might be perceived to influence the results and/or discussion reported in this paper.

References

1. Funfschilling, U.*, et al.* Glycolytic oligodendrocytes maintain myelin and long-term axonal integrity. *Nature* 485, 517-521 (2012).
2. Lee, Y.*, et al.* Oligodendroglia metabolically support axons and contribute to neurodegeneration. *Nature* 487, 443-448 (2012).
3. Miron, V.E.*, et al.* M2 microglia and macrophages drive oligodendrocyte differentiation during CNS remyelination. *Nat Neurosci* 16, 1211-1218 (2013).
4. Ruckh, J.M.*, et al.* Rejuvenation of regeneration in the aging central nervous system. *Cell Stem Cell* 10, 96-103 (2012).
5. Bieber, A.J., Kerr, S. & Rodriguez, M. Efficient central nervous system remyelination requires T cells. *Ann Neurol* 53, 680-684 (2003).
6. Woodruff, R.H., Fruttiger, M., Richardson, W.D. & Franklin, R.J. Platelet-derived growth factor regulates oligodendrocyte progenitor numbers in adult CNS and their response following CNS demyelination. *Mol Cell Neurosci* 25, 252-262 (2004).
7. Arnett, H.A.*, et al.* bHLH transcription factor Olig1 is required to repair demyelinated lesions in the CNS. *Science* 306, 2111-2115 (2004).
8. Ousman, S.S. & David, S. Lysophosphatidylcholine induces rapid recruitment and activation of macrophages in the adult mouse spinal cord. *Glia* 30, 92-104 (2000).
9. Burzyn, D.*, et al.* A special population of regulatory T cells potentiates muscle repair. *Cell* 155, 1282-1295 (2013).
10. Arpaia, N.*, et al.* A Distinct Function of Regulatory T Cells in Tissue Protection. *Cell* 162, 1078-1089 (2015).
11. Kim, J.M., Rasmussen, J.P. & Rudensky, A.Y. Regulatory T cells prevent catastrophic autoimmunity throughout the lifespan of mice. *Nat Immunol* 8, 191-197 (2007).
12. Christiaansen, A.F., Boggiatto, P.M. & Varga, S.M. Limitations of Foxp3(+) Treg depletion following viral infection in DEREG mice. *J Immunol Methods* 406, 58-65 (2014).
13. Meyer Zu Horste, G.*, et al.* Active immunization induces toxicity of diphtheria toxin in diphtheria resistant mice--implications for neuroinflammatory models. *J Immunol Methods* 354, 80-84 (2010).
14. Mayer, C.T.*, et al.* Advantages of Foxp3(+) regulatory T cell depletion using DEREG mice. *Immun Inflamm Dis* 2, 162-165 (2014).
15. Huang, J.K.*, et al.* Retinoid X receptor gamma signaling accelerates CNS remyelination. *Nat Neurosci* 14, 45-53 (2011).
16. Zhang, H., Jarjour, A.A., Boyd, A. & Williams, A. Central nervous system remyelination in culture--a tool for multiple sclerosis research. *Exp Neurol* 230, 138-148 (2011).
17. Hild, W. [Myelin formation in central nervous system tissue cultures]. *Verh Anat Ges* 53, 315-317 (1956).
18. Birgbauer, E., Rao, T.S. & Webb, M. Lysolecithin induces demyelination in vitro in a cerebellar slice culture system. *J Neurosci Res* 78, 157-166 (2004).
19. Ling, C., Verbny, Y.I., Banks, M.I., Sandor, M. & Fabry, Z. In situ activation of antigen-specific CD8+ T cells in the presence of antigen in organotypic brain slices. *J Immunol* 180, 8393-8399 (2008).
20. Kim, J.*, et al.* PINK1 Deficiency Enhances Inflammatory Cytokine Release from Acutely Prepared Brain Slices. *Exp Neurobiol* 22, 38-44 (2013).
21. Sheridan, G.K. & Dev, K.K. S1P1 receptor subtype inhibits demyelination and regulates chemokine release in cerebellar slice cultures. *Glia* 60, 382-392 (2012).
22. Su, B.Y.*, et al.* The expression of ccn3 (nov) RNA and protein in the rat central nervous system is developmentally regulated. *Mol Pathol* 54, 184-191 (2001).
23. Leask, A. & Abraham, D.J. All in the CCN family: essential matricellular signaling modulators emerge from the bunker. *J Cell Sci* 119, 4803-4810 (2006).

24. Lin, C.G*., et al.* CCN3 (NOV) is a novel angiogenic regulator of the CCN protein family. *J Biol Chem* 278, 24200-24208 (2003).
25. Wang, X., He, H., Wu, X., Hu, J. & Tan, Y. Promotion of dentin regeneration via CCN3 modulation on Notch and BMP signaling pathways. *Biomaterials* 35, 2720-2729 (2014).
26. Kotter, M.R., Setzu, A., Sim, F.J., Van Rooijen, N. & Franklin, R.J. Macrophage depletion impairs oligodendrocyte remyelination following lysolecithin-induced demyelination. *Glia* 35, 204-212 (2001).
27. Perbal, B. NOV (nephroblastoma overexpressed) and the CCN family of genes: structural and functional issues. *Mol Pathol* 54, 57-79 (2001).
28. Perbal, B. CCN proteins: A centralized communication network. *J Cell Commun Signal* 7, 169-177 (2013).
29. Le Dreau, G*., et al.* NOV/CCN3 promotes maturation of cerebellar granule neuron precursors. *Mol Cell Neurosci* 43, 60-71 (2010).
30. Xin, L.W., Martinerie, C., Zumkeller, W., Westphal, M. & Perbal, B. Differential expression of novH and CTGF in human glioma cell lines. *Clin Mol Pathol* 49, M91-97 (1996).
31. Raposo, C*., et al.* CNS repair requires both effector and regulatory T cells with distinct temporal and spatial profiles. *J Neurosci* 34, 10141-10155 (2014).
32. Saxena, A*., et al.* Regulatory T cells are recruited in the infarcted mouse myocardium and may modulate fibroblast phenotype and function. *Am J Physiol Heart Circ Physiol* 307, H1233-1242 (2014).
33. Weirather, J*., et al.* Foxp3+ CD4+ T cells improve healing after myocardial infarction by modulating monocyte/macrophage differentiation. *Circ Res* 115, 55-67 (2014).

Figure Legends

Figure 1. T_{reg} are required for efficient OPC differentiation and remyelination *in vivo*

(a) Immunohistochemical analysis of $CC1^+Olig2^+$ cells per lesion area in spinal cords of Foxp3-DTR and C57BL/6 mice at 14 days post lesion (d.p.l.). n = 6 mice in control and n = 5 mice in T_{reg}-depleted groups (t = 2.703, d.f. = 9, **P* = 0.0243; t = 5.624, d.f. = 9, ****P* = 0.0003).

(b) Representative images of **(a)** showing demyelination by luxol fast blue staining (scale bar = 200 µm) and $CC1^+Olig2^+$ cells in lesions (scale bar = 100 µm, green = $Olig2^+$ cells, red = $CC1^+$ cells, blue = DAPI, right panels = merged images).

(c) Lesion size of Foxp3-DTR mice +/- DT at 5 d.p.l. n = 5 mice per group. (t = 1.773, d.f. = 8, P = 0.1142).

(d) $Olig2^+Ki67^+$ cells per lesion area in spinal cords of Foxp3-DTR mice at 5 d.p.l. n = 5 mice per group. (t = 0.7789, d.f. = 8, P = 0.4584).

(e) Electron micrographs showing distribution of remyelinated axons versus unmyelinated axons in spinal cord lesions of control or T_{reg}-depleted mice at 17 d.p.l. Scale bar = 5 µm (top) and 1 µm (bottom). Three mice per group were analyzed (middle panel). Data (right panel) represent mean ± SEM from 109 micrographs from 3 mice per group. Two-tailed Mann-Whitney test. (U = 2, P < 0.0001)

(f) $CC1^+Olig2^+$ cells per lesion area in spinal cords of DT-treated Foxp3-DTR mice with or without adoptively transferred T_{reg} at 14 d.p.l. n = 15 mice in T_{reg}-depleted, n = 8 mice in T_{reg}-depleted/adoptively transferred T_{reg} group pooled from 2 independent experiments. (t = 2.353, d.f. = 21, P = 0.0285).

(g) Representative flow cytometric identification of adoptively transferred T_{reg} in lymph nodes of T_{reg}-injected mice from **(f)** and controls, gated on $CD4^+$ cells.

(h) Immunohistochemical analysis of $CC1^+Olig2^+$ cells per area of the corpus callosum at 2 weeks post-cuprizone withdrawal. n = 5 mice/group, data represent analysis of 1-2 regions of corpus callosum per mouse (t = 2.693, d.f. = 8, P = 0.0274).

(i) Representative images of **(h).** Top: Black Gold II myelin stain. Bottom: $Olig2^+CC1^+$ cell staining (green = $Olig2^+$ cells, red = $CC1^+$ cells, scale bars = 100 μm).

Data shown are representative of 4 **(a,b)**, 2 **(c,d,f,g)** and 1 **(e, h, i)** independent biological experiments. Data presented with mean values indicated, error bars = SEM, unpaired two-tailed Student's *t* test, unless otherwise indicated above. *p<0.05, ***p<0.001.

Figure 2: T_{reg} directly promote brain tissue myelination and remyelination *ex vivo*

(a-c) Analysis of **(a)** MBP^+ cells and **(b)** myelination index per field of view (FOV) in brain stem slices treated with control media or Treg-conditioned media. **(c)** Representative images taken from z-stacks at 7 d.i.v (scale bar = 100 μm, green = NF200, red = MBP). Control: MBP^+ counts n = 17 FOV and myelination index n = 8 FOV. T_{reg}: MBP^+ counts n = 8 and myelination index n = 12 FOV. Fields of view were selected from 3-4 slices/group (MBP^+ counts: $U = 28.5$, $P = 0.0196$, two-tailed Mann-Whitney *U* test; myelination index: $t = 2.886$, d.f. = 18, $P = 0.0098$, unpaired two-tailed Student's *t* test).

(d-f) Analysis of **(d)** MBP^+ cells and **(e)** myelination index per FOV in control, demyelinated and remyelinating brain stem slices. **(f)** Representative images taken from z-stacks (scale bar = 100 μm, green = NF200, red = MBP). Control: MBP^+ counts n = 15 FOV and myelination index n = 10 FOV. Demyelination: MBP^+ counts n = 6 FOV and myelination index n = 6 FOV. Remyelination control: MBP^+ counts n = 5 FOV and myelination index n = 20 FOV. Remyelination+T_{reg}: MBP^+ counts n = 26 and myelination index n = 32 FOV. Fields of view were selected from 3-6 slices/group (MBP^+ counts: demyelination, $U = 0$, $P < 0.0001$, remyelination, $U = 0$, $P < 0.0001$, two-tailed Mann Whitney *U* test; myelination index: demyelination, $U = 9$, $P = 0.0225$, two-tailed Mann Whitney *U* test, remyelination, $t = 5.845$, d.f. = 50, $P = 0.001$, unpaired two-tailed Student's *t* test).

(g-i) Analysis of **(g)** MBP^+ cells and **(h)** myelination index per FOV in brain stem slices. **(i)** Representative images taken from z-stacks (scale bar = 100 µm, green = NF200, red = MBP). Control: MBP^+ counts n = 11 FOV and myelination index n = 10 FOV. T_{reg}: MBP^+ counts n = 13 and myelination index n = 12 FOV. Fields of view were selected from 3-6 slices/group (MBP^+ counts: t = 7.537, d.f. = 22, P < 0.0001; myelination index: t = 2.334, d.f. = 20, P = 0.0301, unpaired two-tailed Student's t tests).

Data shown are representative of 6 **(a-c)** and 2 **(d-f, g-i)** independent experiments. Data presented with mean values indicated, error bars = SEM, *p<0.05, **p<0.01, ***p<0.001.

Figure 3: T_{reg} directly enhance oligodendrocyte differentiation and myelination *in vitro*

(a-d) Immunofluorescence analysis of **(a)** MBP^+ cell numbers (t = 8.200, d.f. = 10, P < 0.0001) **(b)** percentage area (U = 0, P = 0.0022), **(c)** total $Olig2^+$ cell numbers (t = 0.8294, d.f. = 10, P = 0.4263) and **(d)** representative images of mixed glial cultures analyzed (scale bar = 100 µm, green = Olig2, red = MBP), n = 6 wells.

(e,f) Immunofluorescence analysis of **(e)** $Olig2^+Ki67^+$ cell numbers (t = 1.299, d.f. = 10, P = 0.2230) with **(f)** representative images of mixed glial cultures (scale bar = 100 µm, green = Olig2, red = Ki67), n = 6 wells.

(g,h) Immunofluorescence analysis of **(g)** MBP^+ cell numbers (t = 6.431, d.f. = 22, P < 0.0001) and **(h)** representative images of pure OPC cultures analyzed (scale bar = 50 µm, red = MBP, blue = DAPI), n = 12 fields of view.

(i,j) Immunofluorescence analysis of **(i)** MBP^+CC1^+ cell numbers (n.d. = not detectable) and **(j)** representative images of DRG neuron-OPC co-cultures in the presence or absence of T_{reg}-conditioned medium, n = 20 fields of view. Image scale bars = 50 µm and 20 µm (enlarged image), red = MBP, green = CC1, blue = DAPI.

Data shown are representative of at least 12 **(a,b,d)**, 3 **(c,g-j)** and 2 **(e,f)** independent experiments. Data presented with mean values indicated, error bars = SEM, Unpaired, two-tailed, Student's *t* test (cell counts) and Mann-Whitney *U* tests (percentage area), ** P<0.01, *** P<0.001.

Figure 4. CCN3 is produced by T_{reg} and promotes oligodendrocyte differentiation and myelination

(a) ELISA quantification of CCN3 in T cell-conditioned media, n = 4 independently generated supernatants using different mice *(U* = 0, *P* = 0.0294, two-tailed Mann-Whitney *U* test).

(b) Western blot analysis of CCN3 in T_{reg}-conditioned medium. Recombinant CCN3 (rCCN3, 25 ng, R&D Systems) was used as a positive control.

(c,d) Immunofluorescence analysis of **(c)** MBP^+ cell numbers (Control vs T_{reg}: *t* = 3.648, d.f. = 10, *P* = 0.0045; T_{reg} vs T_{reg}+aCCN3: *t* = 6.104, d.f. = 10, *P* = 0.0001, unpaired two-tailed Student *t* test; T_{reg} vs T_{reg}+IgG: *U* = 10, *P* = 0.2207, Mann-Whitney *U* test) and **(d)** MBP^+ percentage area in mixed glial cultures, n = 6 wells (Control vs T_{reg}: *U* = 0, *P* = 0.0022; T_{reg} vs T_{reg}+aCCN3: *U* = 0, *P* = 0.0022, T_{reg} vs T_{reg}+IgG: *U* = 18, *P* = 1, two-tailed Mann-Whitney *U* test). **(e)** Myelination index (MBP^+NF200^+) of brain stem slices at 7 d.i.v. n = 15 FOV for control, T_{reg} and T_{reg}+anti-CCN3 conditions. n = 14 FOV for T_{reg}+IgG condition. Fields of view were from 3-6 slices/group (control vs T_{reg}: *t* = 2.739, d.f. = 28, *P* = 0.0106; T_{reg} vs T_{reg}+anti-CCN3: *t* = 4.998, d.f. = 28, *P* < 0.0001, unpaired two-tailed Student's *t* test).

(f) Immunofluorescence analysis of MBP^+ percentage area in mixed glial cultures, n = 6 wells, (Control vs T_{reg}: *U* = 0, *P* = 0.0022; T_{reg} vs T_{reg} CCN3-depleted: *U* = 3, *P* = 0.0152; T_{reg} CCN3-depleted vs T_{reg} IgG-depleted: *U* = 5, *P* = 0.0411, two-tailed Mann-Whitney *U* test).

(g,h) Immunofluorescence analysis of **(g)** myelination index (MBP^+NF200^+) and **(h)** representative images of brain stem slices at 7 d.i.v., n = 20 FOV for Control, T_{reg}, CCN3-depleted and IgG-depleted conditions; n = 15 FOV for CCN3-eluted condition; n = 13 FOV for IgG-eluted condition. Fields of view were from 3-4 slices/group (control vs T_{reg}: *t* = 5.378, d.f. = 38, *P* < 0.0001; T_{reg} vs CCN3-depleted: *t* =

4.159, d.f. = 38, $P = 0.0002$; CCN3-depleted vs IgG-depleted: $t = 4.446$, d.f. = 38, $P < 0.0001$, unpaired two-tailed Student's *t* test; CCN3-eluted vs IgG-eluted: $U = 43$, $P = 0.0129$, two-tailed Mann-Whitney test). Scale bar = 100 µm, green = NF200, red = MBP.

Data shown are representative of at least 4 **(a)**, 2 **(b, f-h)** and 3 **(c-e)** independent experiments. Data presented with mean values indicated, error bars = SEM, *p<0.05, **p<0.01, ***p<0.001.

Online methods

Animals

All mice were on a C57BL/6 background and were bred in-house. Foxp3-DTR mice were a kind gift from Prof. Alexander Rudensky (Memorial Sloan Kettering Institute, New York) and Foxp3-eGFP mice were a kind gift from Prof. B. Malissen[34]. Experiments used both male and female neonatal P0-P9 pups and animals from 6-16 weeks from sources above. To deplete $Foxp3^+$ cells in Foxp3-DTR mice, diphtheria toxin was administered as described below. All animal maintenance and experiments were in compliance with the UK Home Office and approved by the University's Ethical Committee.

T_{reg} depletion and induction of lysolecithin-mediated demyelination

Male and female mice from 8-18 weeks of age were used. To deplete $Foxp3^+$ cells in Foxp3-DTR mice, 1 µg DT (Sigma) in 200 µl saline was injected i.p. daily for 3-4 days before demyelination. For maintenance of T_{reg} depletion, 1 µg DT was injected i.p. every 3rd day after the demyelination procedure. Control mice were treated with saline. Depletion was routinely confirmed in blood and spleen by flow cytometry. L-α-Lysophosphatidylcholine (lysolecithin; Sigma) was used to induce a focal demyelinated lesion in the spinal cord of mice as described previously[6,35]. In brief, 1.2 µl lysolecithin was injected into the ventral white matter of the lower thoracic spinal cord between vertebrae T11-12 or T12-13. At indicated time points, mice were terminally anesthetized with Ketamin/Rompun, transcardially perfused with 4% paraformaldehyde in PBS or PBS alone (for flow cytometry studies), and spinal cord tissue was dissected.

Adoptive transfer of wild-type T_{reg} into T_{reg}-depleted FoxP3-DTR mice

FoxP3-DTR mice were treated with DT as described above. In the 24 hr prior to lysolecithin-induced demyelination, mice were injected i.p. with $1x10^6$ MACS-purified T_{reg} from wild-type mice that were insensitive to DT treatment using a $CD4^+$ T cell isolation kit (Stemcell Technologies).

Tissue processing

For immunohistochemistry, spinal cord tissue was post-fixed for 2-4 hr in 4% PFA and immersed in 20% sucrose in PBS solution overnight. For cryo-preservation spinal cords were embedded with OCT medium (VWR) and non-consecutive 12 µm thick cryo-sections from the approximate center of lesions were mounted on glass slides[4].

Immunofluorescence staining of CNS tissue

After blocking with 10% goat serum (Vector Laboratories), spinal cord sections were incubated with antibodies for APC (1:100, clone CC1, Abcam), Ki67 (1:200, clone SoIA15, eBioscience), and Olig2 (1:200; cat. no. AB9610, Millipore) overnight. Secondary antibodies goat anti-rabbit AF488 (1:200; cat. no. A-11008, Life Technologies) and goat anti-rat AF594 (1:200; cat. no. A-11007, Life Technologies) were incubated for 1 hr at RT. For CC1 detection acidic antigen retrieval was performed and a mouse-on-mouse immunodetection kit was used (Vector Laboratories). Nuclei were counterstained with DAPI before coverslipping with ProLong Gold Antifade (Life Technologies). Spinal cord images were acquired on a Leica DM5500 epifluorescence microscope.

Luxol Fast Blue staining of spinal cord tissue

Tissue was placed in 1:1 alcohol:chloroform solution for 10 hr before dehydration in alcohol and incubation in 0.1% luxol fast blue solution (Sigma) at 56°C for 16 hr. Tissue was rinsed and differentiated in 0.05% lithium carbonate solution for 30 sec followed by 70% alcohol for 30 sec. After

washing with distilled water tissue was differentiated in 95% alcohol and twice in 100% alcohol (each 5 min) before immersing twice in xylene for 5 min and coverslipping.

Electron Microscopy of spinal cord lesions

Animals were perfused with 3% glutaraldehyde, 2% paraformaldehyde, 0.1M phosphate buffer (pH 7.4), 0.7% (w/v) NaCl and spinal cords were dissected and post-fixed overnight. Specimen were post-fixed in 1% osmium tetraoxide (Agar Scientific, Stansted, UK), dehydrated, stained en bloc with uranyl acetate (Agar Scientific, Stansted, UK), and embedded in Durcupan resin (Sigma-Aldrich, UK). Ultrathin sections (70 nm) were cut on a Leica UCT ultramicrotome with a Diamond knife (Diatome), mounted on formvar-coated copper grids (Electron Microscopy Science), and counterstained with uranyl acetate and lead citrate. Random electron micrographs (35 per animal) were taken from the lesions with a FEI Spirit transmission microscope with a Gatan Orius SC200B Camera. A total of 3399 control axons and 2076 axons from T_{reg}-depleted lesions were analysed blindly.

Flow cytometric immunophenotyping

Fresh spinal cord tissue was dissected following transcardial perfusion with PBS was weighed and placed in Neuro Medium (Miltenyi Biotec). Medium was removed and tissues were individually passed through 70 µm strainers, washed with 30% percoll to pellet cells and myelin-containing supernatant was carefully removed. Cells were resuspended in 200 µl flow cytometry staining buffer (FCSB; 1% FCS, 0.01% NaN_3 in PBS) prior to cell surface staining with antibodies to CD45 (clone 104; 1:400), CD11b (clone M1/70; 1:400), CD3 (clone 145-2C11; 1:200) and CD4 (clone GK1.5; 1:200). Foxp3 expression was determined in fresh cells from Foxp3-eGFP or Foxp3-GFP-DTR mice. To calculate cell numbers, singlets were identified by FSC-H vs FSC-A, and $CD45^+$ cells were gated for subsequent analyses of CD11b, CD3, CD4 and Foxp3-eGFP. All flow cytometry antibodies were from eBioscience. Data were acquired on a FACSCanto II and analyzed using FlowJo software.

Cuprizone-induced demyelination

Eleven-week-old male C57BL/6 and FoxP3DTR mice were fed with 0.2% cuprizone [bis(cyclohexanone) oxaldihydrazone], (Teklad Custom Diet TD.140804, Envigo]. Food and water were available *ad libitum*. Cuprizone feeding was maintained for 25 days to induce demyelination. Diet was then changed to normal rodent chow for additional 2 weeks to allow remyelination to occur. To deplete T_{reg}, mice were injected with DT (0.04g DT/Kg) or vehicle on day 24 and day 25. T_{reg} depletion was maintained by DT administration every three days. Mice were sacrificed on day 39 and were perfused transcardially with PBS followed by cold 4% paraformaldehyde. Brains were removed, postfixed overnight in 4% paraformaldehyde and cryoprotected in 30% sucrose. Coronal frozen sections of 20 µm thickness were cut using a Leica cryostat. Sections between 1 mm and -1 mm relative to Bregma were collected and stained for CC1 and Olig2 as described above. The number of mature oligodendrocytes in the corpus callosum was quantified on images of 1-2 sections per animal with five animals per group. Images of the midline segment of the corpus callosum from frontal and middle sections were used to delineate the area for analysis of Olig2/CC1 positive cells.

Black Gold II staining

Tissue sections were stained with Black Gold II (AG105, Millipore Corp, Billerica, MA) according to manufacturer's instructions. Briefly, sections were washed in water, immersed in pre-warmed Black Gold II solution and incubated at 60°C for 15 min followed by transfer into pre-warmed 1% sodium thiosulfate at 60°C for 5 min. Slides were rinsed three times, dehydrated, immersed in xylene for 2 min and coverslipped with mounting media.

Gene expression analyses

For qPCR, total RNA was extracted from the cerebella of perfused mice with an RNeasy FFPE kit (Qiagen) using a modified protocol. Tissue was homogenised in supplied PKD buffer before treatment with proteinase K. All subsequent steps were followed according to manufacturer's instructions. RNA purity and concentration was assessed by Nanodrop spectrophotometry. Samples were treated with DNase I (Invitrogen) prior to reverse transcription with Superscript IV (Invitrogen). cDNA samples were assayed in triplicate by qPCR using Fast SYBR Green (ThermoFisher Scientific) on a Roche LightCycler 480 system. Relative gene expression of *Plp1* gene was determined with the Pfaffl method using *Gapdh* as internal control[36] . Primer sequences were as previously described[37]. An unpaired, two-tailed Student's t test was performed to assess statistical differences on delta Ct values of each condition, with a significance threshold of 0.05.

In situ hybridization of proteolipid protein (PLP) mRNA on paraformaldehyde-fixed CNS tissue was performed as previously described[38]. The plasmid containing a fragment of 801bp *Plp* cDNA was provided by Prof I Griffith (University of Glasgow). Briefly, sections were incubated with digoxigenin-labeled complementary RNA probes at 65°C overnight and subjected to a standard wash protocol (50% formamide, 1× standard saline citrate, 0.1% Tween-20, 65°C, 3× 30 minutes) to remove nonspecific probe binding. The target bound probes were detected by alkaline phosphatase–conjugated antidigoxigenin antibody, and visualized as purple precipitate after incubation in NBT/BCIP solution according to the manufacturer's instructions (Roche, Lewes, UK). The slides were dehydrated with ascending concentration of ethanol, cleared with xylene, and mounted in dibutyl phthalate in xylene. Images were acquired with the Zeiss Axio Observer microscope.

T cell culture

$CD4^+$ T cells were immunomagnetically purified by negative selection (Stem Cell Technologies) from splenocytes of 6-14 week old male and female C57BL/6 mice and cultured in RPMI 1640 (Life Technologies) supplemented with 10% FCS, 1% penicillin/streptomycin, 1% L-glutamine, 1% Hepes, 1% sodium pyruvate, 1% non-essential amino acids and 50 nM β-mercaptoethanol (all Life

Technologies). In Supplementary Fig 3d, naïve $CD4^+$ T cells were purified using EasySep™ Mouse Naïve $CD4^+$ T Cell Isolation Kits (Stem Cell Technologies). T cells were activated with plate bound anti-CD3 (1 µg/ml, clone 145-2C11) and soluble anti-CD28 (1 µg/ml, clone 37.51) (both eBioscience) for 3 days in non-polarizing (NP; no exogenous cytokine) or T_{reg}-polarizing conditions consisting of rhTGF-β (2 ng/ml, R&D Systems), rhIL-2 (10 ng/ml, eBioscience) and anti-IFN-γ (10 µg/ml, clone XMG1.2, Bioxcell). T cells were then reactivated in brain slice medium (described below) for a further 72 hr and conditioned media were harvested. Polarization of all cultures was verified by flow cytometry and T_{reg} cultures used for experiments generally consisted of 80-90% $Foxp3^+$ T cells (see Supplementary Fig. 2 f). For CCN3 immunoblotting, depletion and elution, cells were reactivated in serum-free X-VIVO 15 medium (Lonza).

For adoptive transfer experiments, nT_{reg} were immunomagnetically purified (Stem Cell Technologies) by negative selection of $CD4^+$ T cells followed by positive selection of $CD25^+$ cells from splenocytes and lymph nodes of C57BL/6 mice. For i.p. injection, cells were resuspended at $5x10^6$ cells/ml in saline.

Organotypic brain slice culture

Brain stem slices (300 µm) from male and female P0-2 C57BL/6 pups were prepared using a McIlwain Tissue Chopper and cultured in transwell inserts with brain slice medium consisting of 46.6% minimum essential medium, 25% Earle's balanced salt solution, 25% heat inactivated horse serum, 1% penicillin/streptomycin, 1% glutamax (Life Technologies) and 1.4% D-glucose (Sigma). Slices were treated with 5% T cell-conditioned media and/or anti-CCN3 (10 µg/ml; clone 231216, R&D Systems) and/or isotype control (clone 54447, R&D Systems) and/or eluate from immunoprecipitations every other day for the period defined. For remyelination studies, brain stem slices were demyelinated after 14 days in culture with lysolecithin (0.5 mg/ml, Sigma) for 16 hr. Slices were washed and allowed to remyelinate for up to 14 days. For co-culture studies, $1.7x10^4$ FACS-purified natural T_{reg} from Foxp3-eGFP mice were added directly on to brain stem slices in a volume of 10 µl (Supplementary Fig. 2 a).

Staining of organotypic brain slices

Slices were fluorescently stained for myelin basic protein (MBP; 1:600, clone 12, Millipore) and axonal neurofilament-200 (NF200; 1:200, clone RT97, Millipore). After fixation in 4% paraformaldehyde for 45 min at RT, slices were blocked and permeabilized at RT for 1 hr in 3% heat-inactivated horse serum (Life Technologies), 2% bovine serum albumin (Sigma) and 0.5% Triton X-100 (Sigma). Both primary and secondary antibodies (goat anti-rat AF594, cat. no. A11007, goat anti-mouse AF488 cat # A11001 and goat anti-mouse AF405 cat # A31553, 1:500; Life Technologies) were incubated overnight at 4^{o}C. Slices were mounted with ProLong Gold Antifade (Life Technologies) and imaged with a Leica TCS SP5 confocal microscope at 0.5 µm intervals over 10 µm, taking up to 5 fields of view (FOV) per slice, dependent on slice size. Representative images were displayed with a green look up table (LUT) for NF200 and red LUT for MBP, applied using Leica AF software.

Electron microscopy of organotypic brain slices

Slices were immersion fixed in 4% PFA/2% glutaraldehyde in 0.1M phosphate buffer for 24 hr, washed in phosphate buffer and post-fixed in 1% osmium tetroxide in 0.1 M phosphate buffer for 45 min. Samples were dehydrated in increasing concentrations of acetone and embedded in Araldite resin. Ultrathin 60 nm sections were stained in uranyl acetate and lead citrate and then viewed in a JEM1400 Transmission electron microscope (JEOL). To count the percentage of myelinated fibres per unit area of slice (at least 600 µm^2/condition), three photographs were taken from random, non-overlapping fields from each of 3 slices per condition and analyzed. To measure g-ratios, at least 35 randomly chosen axons from each of 3 slices per condition were analyzed by tracing the axonal circumference and the whole fibre circumference (using a graphics pad and pen). G-ratios were calculated by dividing these values and data were analyzed using one-way ANOVA with Bonferroni post-test with $p < 0.05$ considered significant.

Mixed glial cultures

Mixed glial cells were generated from male and female P2-7 C57BL/6 pups according to the protocol of the Neural Tissue Dissociation Kit (P) (Miltenyi Biotec). In short, brains were dissected, cerebellum and meninges were removed and tissue was dissociated via mechanical and papain enzyme digestion prior to filtration through a 40 µm strainer. Cells were plated in poly-L-lysine-coated (10 µg/ml, Sigma) 96 well flat, glass-bottomed plates (BD Falcon) at a density of 10^5 cells per well and cultures were maintained at 37˚C, 5% CO_2. Cells were cultured for 5 days in DMEM (Life Technologies) supplemented with PDGFαα (10 ng/ml; PeproTech), 10% endotoxin-free FCS, 1% penicillin/streptomycin and 1% L-glutamine (Life Technologies). Cells were cultured for a further 2 days in neural medium (Miltenyi Biotec) supplemented with 1% penicillin/streptomycin, 1% L-glutamine, 2% B27/MACS Neuro Brew21 (Miltenyi Biotec) and PDGFαα (10 ng/ml; PeproTech). At day 7 in culture, PDGFαα was withdrawn to allow oligodendrocyte differentiation and cells were stimulated with 5% T_{reg}-conditioned media, rCCN3, anti-CCN3 (clone 231216) or isotype control (clone 54447) (all R&D Systems) or controls for up to 5 days.

Immunofluorescence staining of mixed glial cultures

Cell cultures were fixed in 4% paraformaldehyde (pH 7.4) for 15-20 min at RT and blocked in 10% normal goat serum with 0.1% Triton-X-100 for 1 hr. Cells were then incubated with primary antibody overnight at 4˚C and in secondary antibodies for 1 hr at RT. Cells were counterstained with DAPI for 5 min at RT. Primary antibodies used were rabbit anti-mouse Olig2 (1:200; cat. no. AB9610, Millipore), rat anti-mouse MBP (1:200; clone 12, Millipore), rat anti-mouse Ki67 (1:200; clone SoIA15, eBioscience), rabbit anti-mouse GFAP (1:200; cat. no. Z0334, Dako) and rat anti-mouse CD11b (1:200; clone M1/70, eBioscience) and secondary antibodies used were goat anti-rabbit AF488 (1:1000; cat. no. A-11008) and goat anti-rat AF594 (1:1000; cat. no. A-11007; both Life Technologies). For live/dead staining unfixed cells were stained using the LIVE/DEAD® Viability/Cytotoxicity Kit for mammalian cells (Life Technologies). Immunofluorescence was detected using an EVOS microscope at 10X

magnification, and n = 6 wells per condition, with one mean value from multiple images calculated for each well.

OPC purification

Immunopanning purification of OPC was performed as previously described[39]. Briefly, OPC were purified from male and female P7–9 mouse brain cortices. Tissue culture dishes were incubated overnight with goat IgG and IgM secondary antibodies to mouse (cat. no. 115-005-004, Jackson Laboratories) in 50 mM Tris-HCl at a final concentration of 10 µg/ml, pH 9.5. Dishes were rinsed and incubated at room temperature (RT) with primary antibodies for Ran-2, GalC and O4 from hybridoma supernatants[39]. Rodent brain hemispheres were diced and dissociated with papain (Worthington) at 37°C. After trituration, cells were resuspended in a panning buffer (0.2% BSA in DPBS) and incubated at RT sequentially on three immunopanning dishes: Ran-2 and GalC were used for negative selection before positive selection with O4. OPC were released from the final panning dish using 0.05% Trypsin (Invitrogen). OPCs were typically 95% pure after immunopanning, with a viability of 94%.

OPC–DRG co-cultures

OPC-DRG co-cultures were prepared as previously described[39]. Briefly, DRG neurons from E15 Sprague-Dawley rats were dissociated, plated (150,000 cells per 25 mm cover glass) and purified on collagen-coated coverslips in the presence of 100 ng/ml NGF (AbD Serotec). Neurons were maintained for 3 weeks and washed with DMEM (Invitrogen) extensively to remove any residual NGF before seeding OPC. Co-cultures were grown in chemically defined medium composed of DMEM (Invitrogen) supplemented with B27 (Invitrogen), N2 (Invitrogen), penicillin-streptomycin (Invitrogen), N-acetyl-cysteine (Sigma-Aldrich) and forskolin (Sigma-Aldrich).

CCN3 quantification and depletion

Proteome profiling of conditioned media was performed using an Angiogenesis Antibody Array (R&D Systems) as per manufacturer's instructions, which identified CCN3 as a candidate protein of interest. Levels of CCN3 in T cell-conditioned media were quantified by ELISA (R&D Systems) according to manufacturer's instructions.

T_{reg}-conditioned media were depleted of CCN3 using monoclonal anti-CCN3 antibody-coupled magnetic beads (clone 231216, R&D Systems and Thermo Scientific) or isotype control-coupled beads (clone 54447). Coupling of antibody and beads was performed according to manufacturer's instructions. In short, 1 mg of beads was incubated with 500 µg/mL of antibody solution and the flow-through was analysed by spectrophotometry. For immunoprecipitation, up to 1 ml of T_{reg}-conditioned media were added to 1 mg of monoclonal antibody-coupled magnetic beads and incubated on a rotator at RT for 2 hr with additional vortexing of the samples every 15 min to ensure that the beads remained in suspension. The samples were then placed in a magnetic stand and CCN3-depleted T_{reg}-conditioned media and isotype-treated controls were collected. To elute T_{reg}-derived CCN3, beads were washed and elution buffer (0.1 M glycine, pH 2.0) was added for 3-5 min at RT. To neutralize the low pH of the solution, neutralization buffer (1 M Tris, pH 7.4) was immediately added, samples were placed on a magnetic stand, and the eluate containing T_{reg}-derived CCN3 was collected and resuspended in medium according to initial volume. Eluted product from anti-CCN3-coated and IgG-coated beads was added to brain slice cultures as indicated.

Immunoblotting of CCN3

T cell-conditioned media or recombinant CCN3 (R&D Systems) were enriched for CCN3 using heparin-sepharose beads as previously described[40]. In short, up to 10 ml of T_{reg}-conditioned media (equivalent to 25 ng of CCN3), or recombinant CCN3 were added to 100 µl 50% heparin-sepharose slurry and incubated on a rotator at 4°C overnight. 50 µl of PBS-washed CCN3-bound heparin-sepharose beads and 12.5 µl 5x reducing loading dye were boiled for 10 min prior to loading on a reducing 15% SDS-PAGE. Following transfer onto PVDF membrane (Millipore) and blocking (3% BSA in PBS/1% Tween)

for 1 hr at RT, protein was probed using polyclonal anti-CCN3 antibody (1:1000; cat. no. AF1976, R&D Systems) overnight at 4°C and secondary anti-goat HRP (1:3000; cat. no. sc-2020, Santa Cruz) for 1 hr at RT.

Image analysis and data processing

Customized ImageJ[41] plugins were used to assist quantifying positively stained cells and areas in all models.

Regions of interest corresponding to spinal cord lesions were initially drawn using the polygon tool. Regions were subsequently refined based on the local cell density by thresholding a Gaussian-smoothed duplicate of the DAPI channel to give a more detailed contour which was corrected manually if necessary using a brush selection tool. Cells were then counted manually within the lesion; in some cases counts were automatically initialized as localized regions of high fluorescence detected by the 'find maxima' command of ImageJ before manual verification and correction to ensure that all regions contributing to the final counts were consistent with expected cell morphology (i.e. no artefacts). ImageJ plugins were written to perform the lesion refinement and to assist with manual cell counting.

Myelination index was used for overlap of myelin and axonal markers in 3D, indicating (re)myelination. Confocal z-stacks of brain slices, both red (MBP) and green (NF200) channels were pre-processed by first smoothing with a 3D isotropic Gaussian filter (sigma = 0.5 µm) before subtracting a background estimate created by applying a 3D morphological opening (filter radius = 1 µm). The processed channels were then thresholded, where the threshold was determined automatically by implementation of the 'triangle' method of ImageJ. The overlap coefficient was determined as the proportion of above-threshold pixels in the green channel that were also detected in the red channel, which quantified MBP signals co-localizing with NF200 signals. An ImageJ plugin was written to fully automate the above steps. MBP^+ oligodendrocytes were counted manually.

Cell counts of Olig2$^+$, MBP$^+$ and Ki67$^+$ cells in mixed glial cultures were performed manually. MBP$^+$ areas were determined from the number of above-threshold pixels after applying a small median filter (radius = 1.5 pixels), followed by subtracting a background image generated by the 'subtract background' command of ImageJ (sliding paraboloid option, radius = 100 pixels). For each plate the threshold was determined and the same threshold was applied to all analyzed images within each experiment. An ImageJ plugin was written to automate the above steps. Plugin codes will be made publically available on the Queen's University Belfast website.

Experimental designs and statistical analyses

No statistical methods were used to pre-determine sample sizes but sample sizes were similar to those reported in previous publications[3,15,39]. For *in vivo* studies, any animal that reached a pre-defined welfare limit before the analysis time-point was excluded from the study. For organotypic brain slice experiments, slice integrity was determined by neurofilament 200 staining prior to analysis. Animals and brain slices were randomly assigned to experimental groups at the beginning of experiments. Myelination indices (brain slices) and MBP area (glial cultures) were blindly assessed by a computer programme and in an identical manner for all files. MBP$^+$ cell counts in brain slices were performed by independent observers on randomly selected images from z-stacks. For all other studies, data collection and analyses were not performed blind to the conditions of the experiments. Datasets were tested for normal distribution, variances and statistical significance using unpaired, two-tailed, Student's *t*-tests for parametric data with or without Welch correction, or Mann-Whitney tests for non-parametric data, detailed in legends. Normality of datasets was tested using the KS or D'Agostino-Pearson omnibus normality test methods. Where n was not sufficient for normality testing, non-normal distribution was assumed and non-parametric statistical testing was used. All statistical analysis and graphing of data were performed using GraphPad Prism. Species validation information for antibodies can be obtained from the commercial suppliers indicated.

Data and code availability

The data and analysis code that support the findings of this study are available from the corresponding author upon reasonable request.

Methods-only References

34. Wang, Y.*, et al.* Th2 lymphoproliferative disorder of LatY136F mutant mice unfolds independently of TCR-MHC engagement and is insensitive to the action of Foxp3+ regulatory T cells. *J Immunol* **180**, 1565-1575 (2008).

35. Hall, S.M. The effect of injections of lysophosphatidyl choline into white matter of the adult mouse spinal cord. *J Cell Sci* **10**, 535-546 (1972).

36. Pfaffl, M.W. A new mathematical model for relative quantification in real-time RT-PCR. *Nucleic Acids Res* **29**, e45 (2001).

37. Liu, J.*, et al.* Impaired adult myelination in the prefrontal cortex of socially isolated mice. *Nat Neurosci* **15**, 1621-1623 (2012).

38. Zhao, C., Li, W.W. & Franklin, R.J. Differences in the early inflammatory responses to toxin-induced demyelination are associated with the age-related decline in CNS remyelination. *Neurobiol Aging* **27**, 1298-1307 (2006).

39. Mei, F.*, et al.* Micropillar arrays as a high-throughput screening platform for therapeutics in multiple sclerosis. *Nat Med* **20**, 954-960 (2014).

40. Chevalier, G.*, et al.* novH: differential expression in developing kidney and Wilm's tumors. *Am J Pathol* **152**, 1563-1575 (1998).

41. Schneider, C.A., Rasband, W.S. & Eliceiri, K.W. NIH Image to ImageJ: 25 years of image analysis. *Nat Methods* **9**, 671-675 (2012).

Figure 1

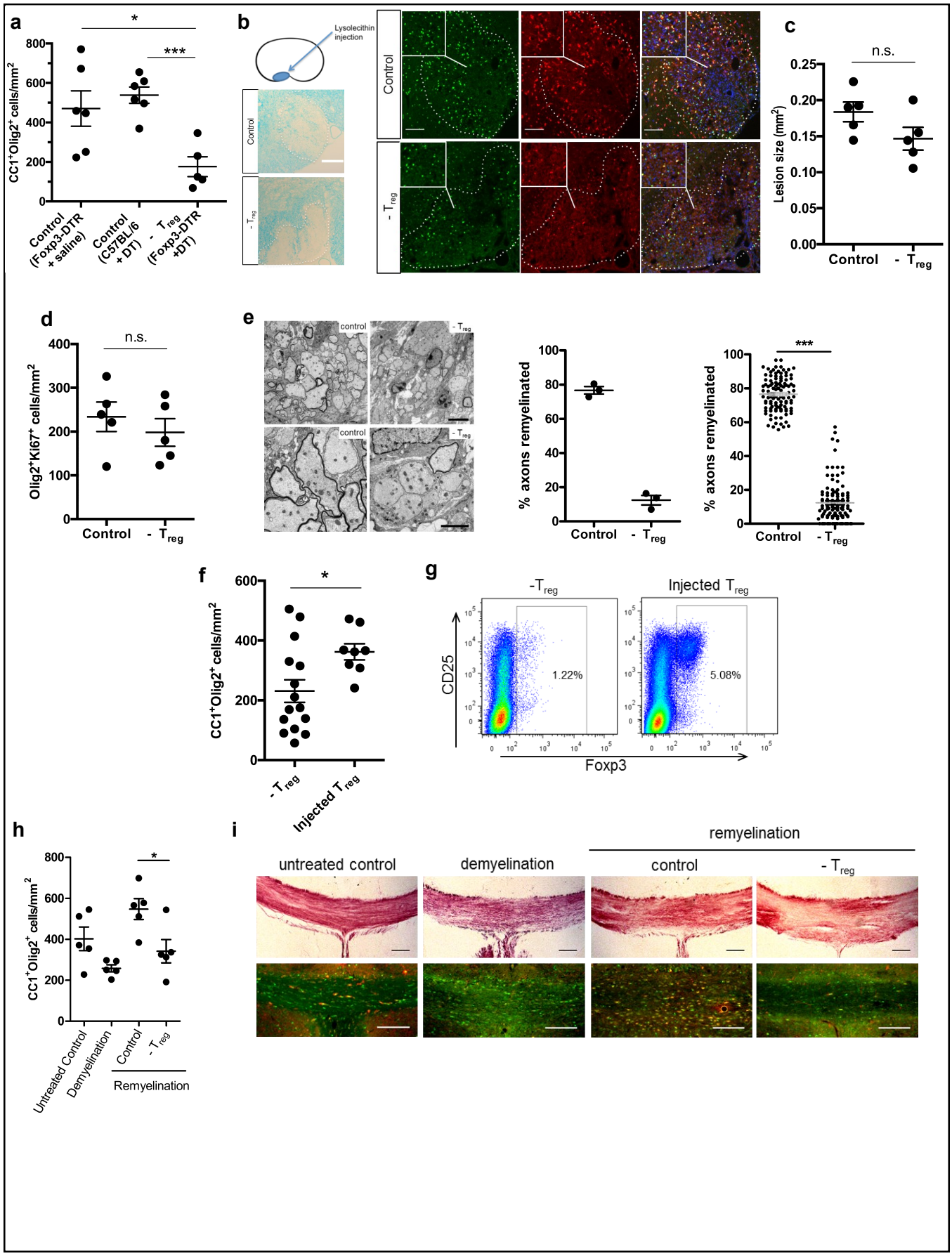
a
b
c
d
e
f
g
h
i
Lysolecithin injection
Control
- Treg
n.s.
Lesion size (mm²)
Olig2⁺Ki67⁺ cells/mm²
% axons remyelinated
CC1⁺Olig2⁺ cells/mm²
-Treg
Injected Treg
CD25
Foxp3
1.22%
5.08%
Untreated Control
Demyelination
Remyelination
untreated control
demyelination
remyelination

Figure 2

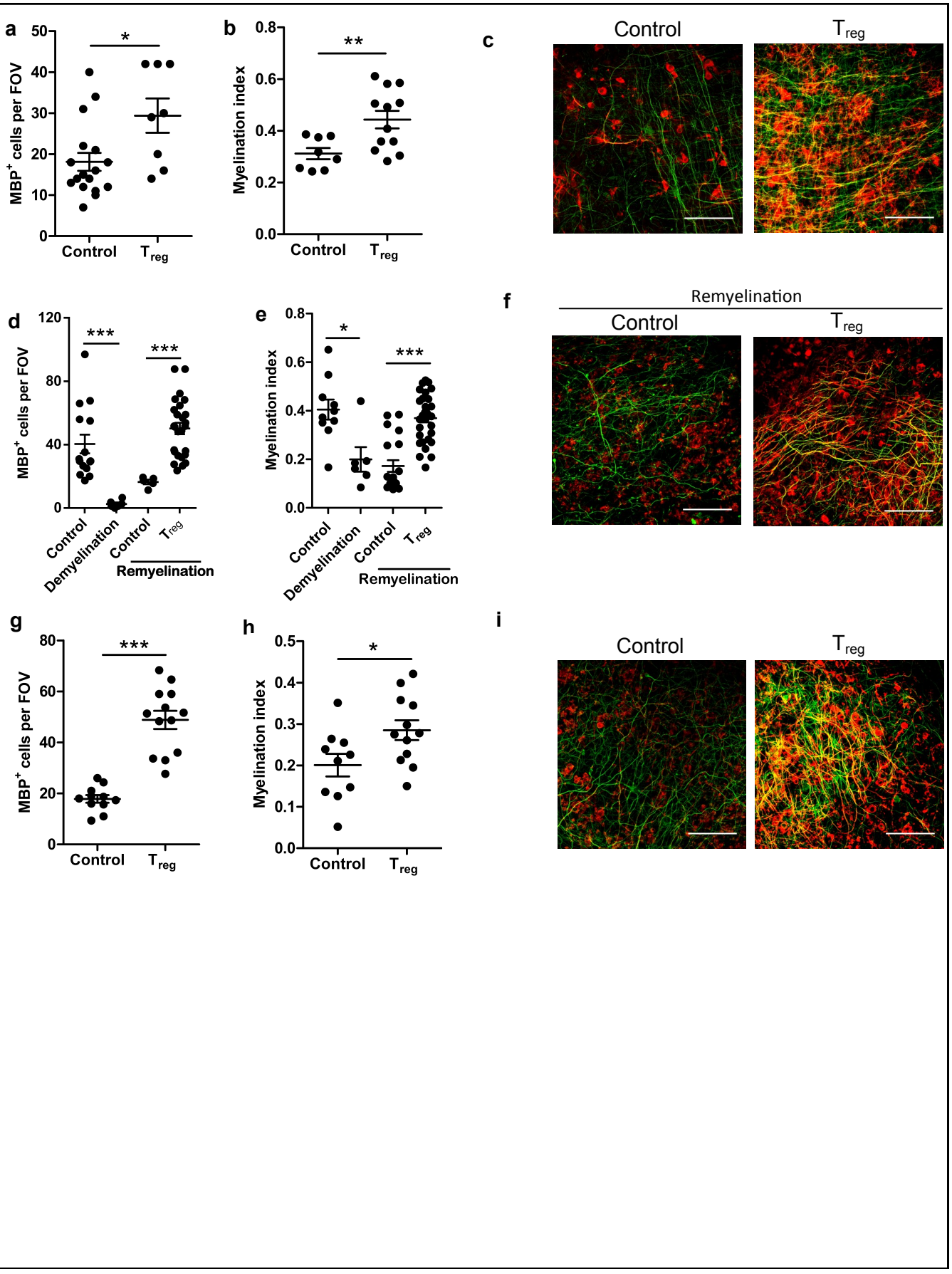
a
MBP+ cells per FOV
Control
Treg
b
Myelination index
c
Control
Treg
d
MBP+ cells per FOV
Control
Demyelination
Remyelination
e
Myelination index
f
Remyelination
g
MBP+ cells per FOV
h
Myelination index
i

Figure 3

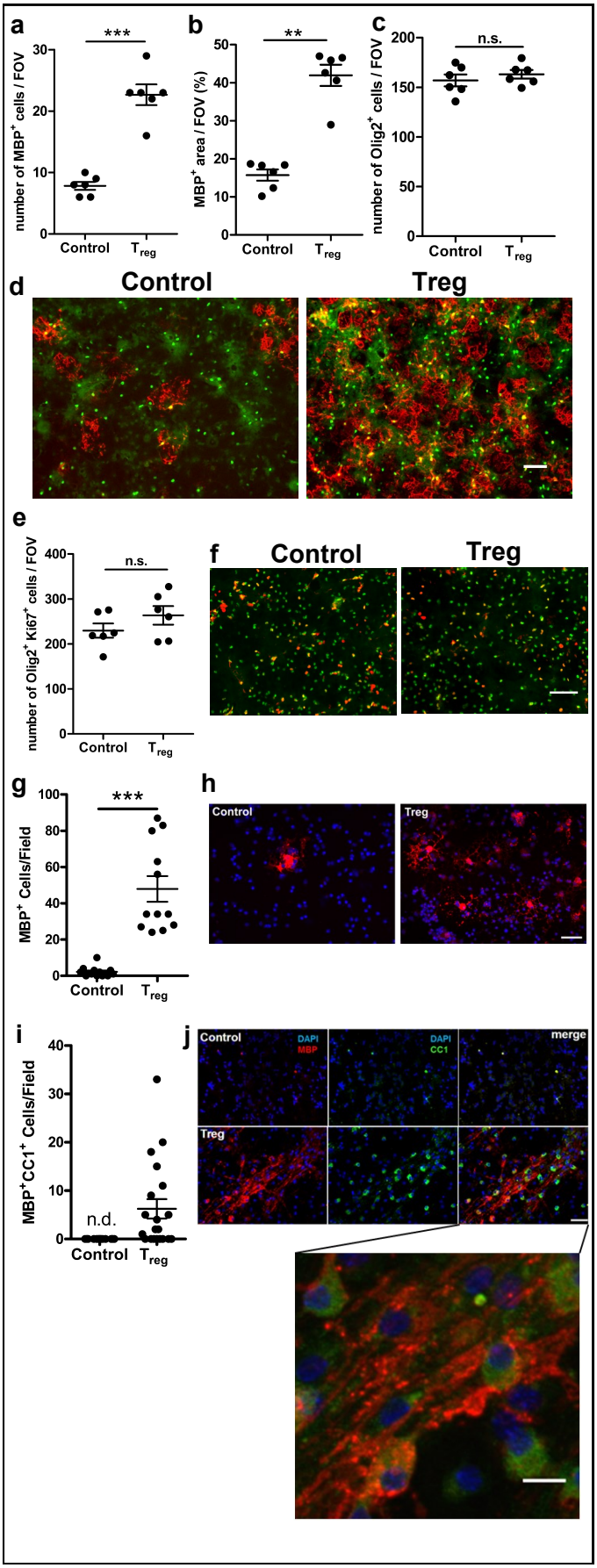
a
***
number of MBP+ cells / FOV
Control
Treg
b
**
MBP+ area / FOV (%)
c
n.s.
number of Olig2+ cells / FOV
d
Control
Treg
e
n.s.
number of Olig2+ Ki67+ cells / FOV
f
Control
Treg
g
***
MBP+ Cells/Field
h
Control
Treg
i
n.d.
MBP+CC1+ Cells/Field
j
Control
DAPI
MBP
DAPI
CC1
merge
Treg

Figure 4

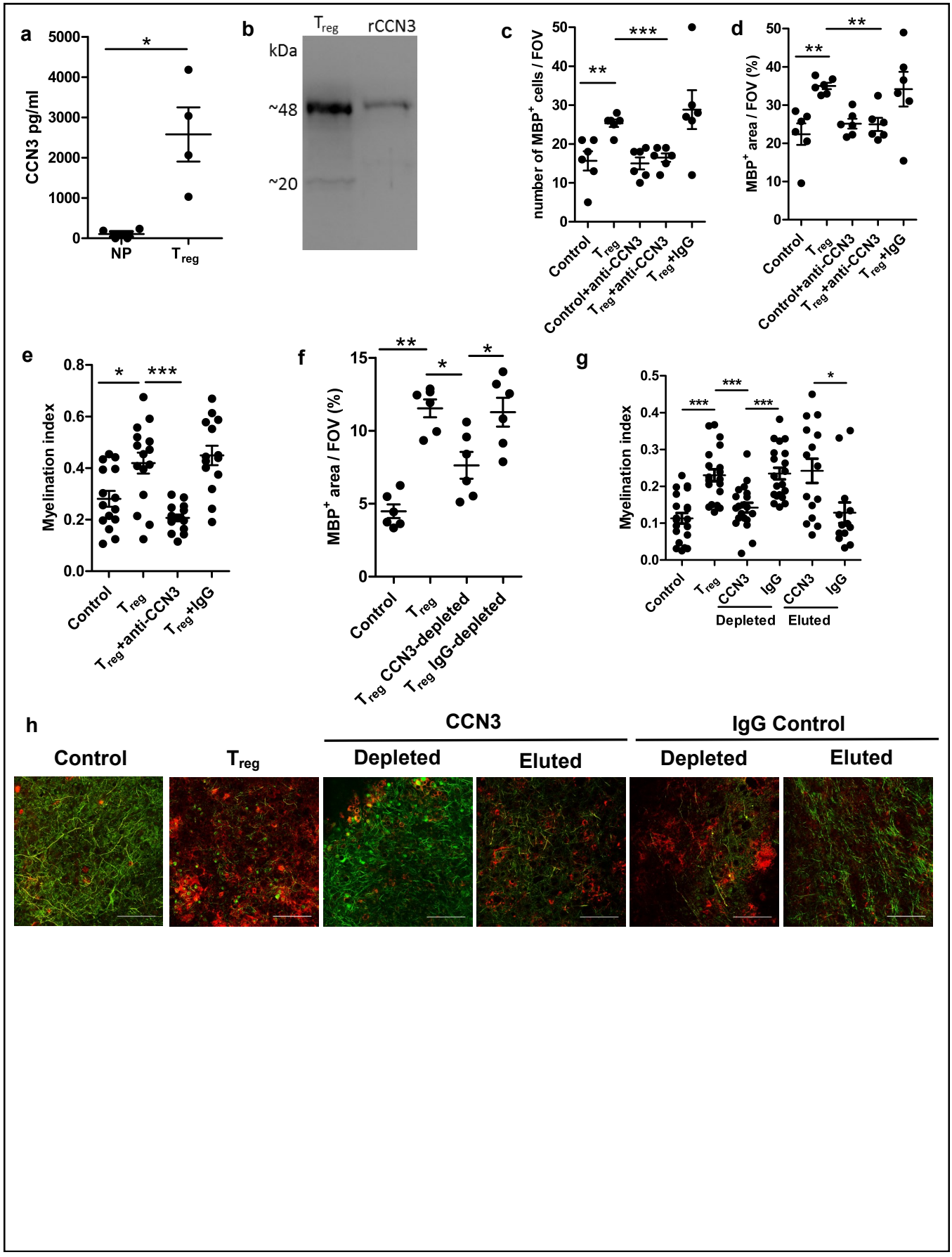
a
CCN3 pg/ml
NP
Treg
b
Treg
rCCN3
kDa
~48
~20
c
number of MBP+ cells / FOV
Control
Treg
Control+anti-CCN3
Treg+anti-CCN3
Treg+IgG
d
MBP+ area / FOV (%)
e
Myelination index
f
MBP+ area / FOV (%)
Treg CCN3-depleted
Treg IgG-depleted
g
Myelination index
CCN3
IgG
Depleted
Eluted
h
Control
Treg
CCN3
IgG Control
Depleted
Eluted

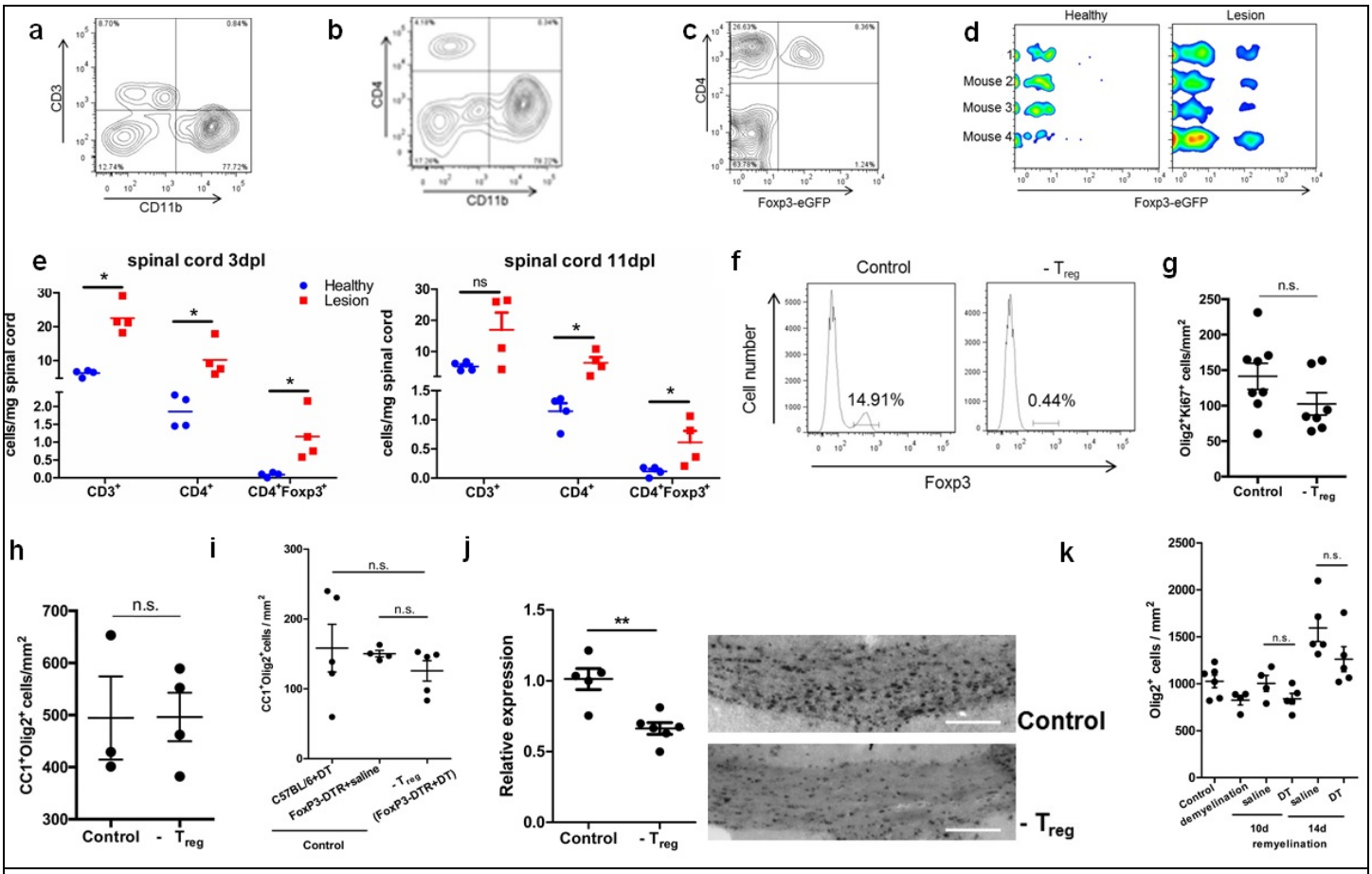

Supplementary Figure 1.

Immunophenotyping and oligodendroglial analysis following lysolecithin- and cuprizone-induced demyelination

(a-d) Representative images of flow cytometric analysis of **(a)** $CD3^+$ T cells, **(b)** $CD4^+$ T cells and **(c,d)** $CD3^+CD4^+Foxp3^+$ T_{reg}, in lesional spinal cord tissue at 3 d.p.l. gated on **(a,b)** $CD45^+$ cells, **(c)** $CD45^+CD3^+$ and **(d)** $CD45^+CD3^+CD4^+$ cells. **(e)** Quantitative immunophenotyping of T cell populations in matched healthy and lesioned spinal cord harvested at 3 and 11 d.p.l., gated on $CD45^+$ cells. n = 4 mice per group. Healthy vs. lesion on 3 d.p.l. on left panel: ($CD3^+$, U = 0, P = 0.0286), ($CD4^+$, U = 0, P = 0.0286), ($CD4^+Foxp3^+$, U = 0, P = 0.0294). Healthy vs. lesion on 11 d.p.l. on right panel: ($CD3^+$, U = 2, P = 0.1143), ($CD4^+$, U = 0, P = 0.0286), ($CD4^+Foxp3^+$, U = 0, P = 0.0294), all two-tailed Mann Whitney U tests. **(f)** Representative flow cytometric analysis of $Foxp3^+$ T_{reg} cells in fresh spleen from DT-treated C57BL/6 (control) and Foxp3-DTR mice (- T_{reg}) at 14 d.p.l., gated on $CD4^+$ cells. **(g)** $Olig2^+Ki67^+$ cells per lesion area in spinal cord of Foxp3-DTR mice at 10 d.p.l. with n = 8 animals in control and n = 7 animals in T_{reg}-depleted groups. (t = 1.580, d.f. = 13, P = 0.1382, unpaired two-tailed Student's t test). **(h)** $CC1^+Olig2^+$ cells per lesion area at 10 d.p.l. in spinal cord of mice, with T_{reg} depletion restricted to pre-lesioning phase, with n=3 animals in control and n=4 animals in T_{reg}-depleted groups. (U = 6, P > 0.9999, two-tailed Mann Whitney U test). **(i)** Immunohistochemical analysis of $CC1^+Olig2^+$ cells per lesion area of the corpus callosum at 10 days post-cuprizone withdrawal. n = 5 animals for C57BL/6 DT-treated controls, n = 4 animals for saline-treated Foxp3-DTR controls, n = 5 animals for T_{reg}-depleted Foxp3-DTR group; data represent analysis of 2-4 regions of corpus callosum per animal (C57BL/6+DT vs FoxP3-DTR+DT: t = 0.8753, d.f. = 8, P = 0.4069, unpaired two-tailed Student's t test; FoxP3-DTR+saline vs FoxP3-DTR+DT: U = 6, P = 0.4127, two-tailed Mann Whitney U test). **(j)** *Plp1* expression analysis in cerebellar tissue of control and T_{reg}-depleted animals at 14 days post-cuprizone withdrawal by qPCR (left panel, normalized to *Gapdh*) and by *in situ* hybridization in corpus callosum (right panel, representative images). n = 5 animals (control) and n = 6 animals in T_{reg}-depleted group (t = 8.684, d.f. = 9, P < 0.0001, unpaired two-tailed Student's t test). **(k)** Immunohistochemical analysis of total $Olig2^+$ cells per lesion area in the corpus callosum at 10 and 14 days post-cuprizone withdrawal. n = 6 animals (control), n = 4 animals (demyelination and 10 days control remyelination group), n=5 (all other remyelination groups); data represent analysis of 2-4 regions of corpus callosum per animal (10 days remyelination: U = 5, P = 0.2857, two-tailed Mann Whitney U test; 14 days remyelination: t = 1.701, d.f. = 8, P = 0.1273, unpaired two-tailed Student's t test). Data shown are representative of at least 3 (**a-d, f**), 2 (**e**, left panel) or 1 (**e**, right panel, **g-k**) independent experiments. Data presented with mean values indicated, error bars = SEM, *P<0.05, ***P<0.001.

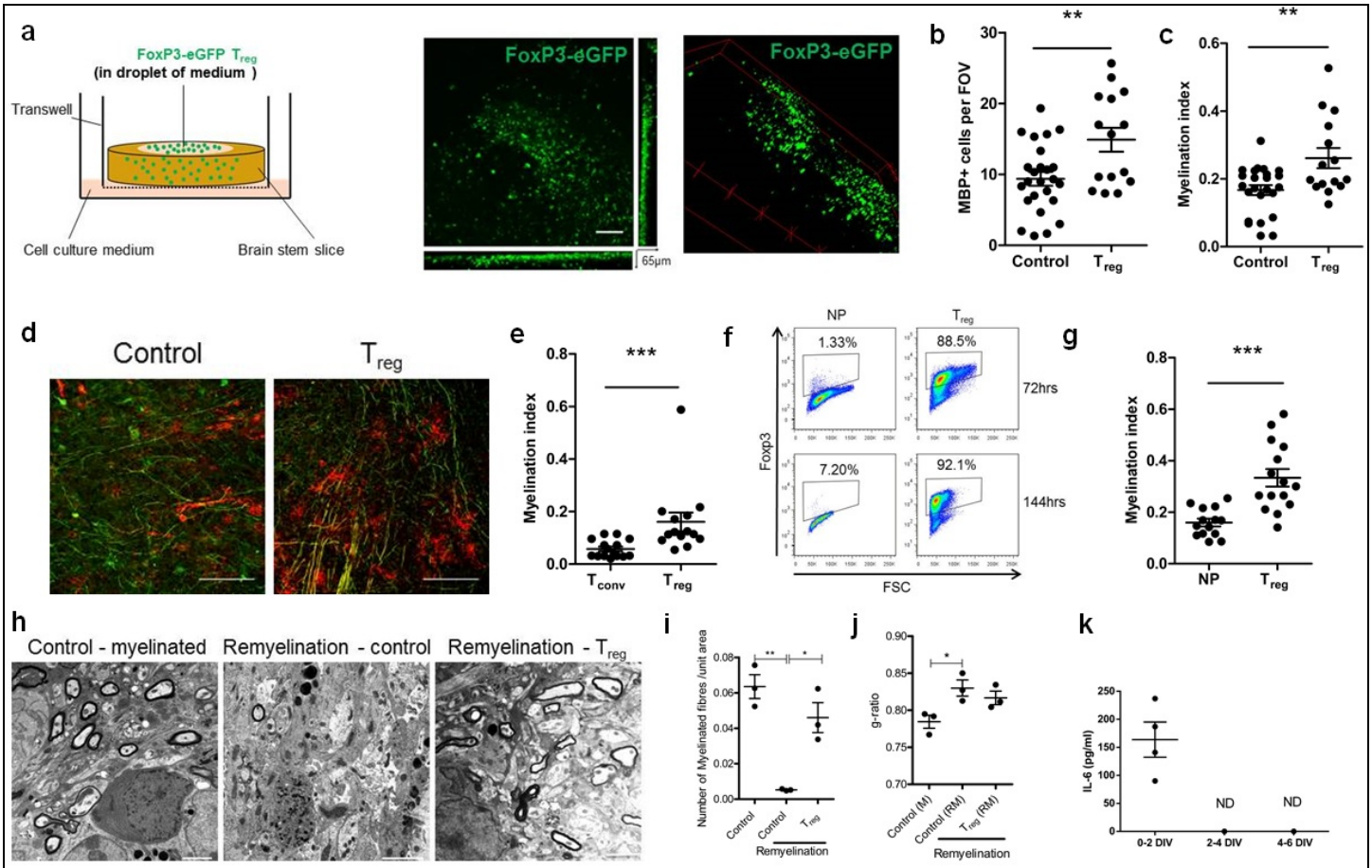

Supplementary Figure 2

T_{reg} and T_{reg}-conditioned media promote brain slice myelination and remyelination

(a) Schematic diagram and 3D image of Foxp3-eGFP$^+$ T_{reg} in organotypic brain slice cultures representing z-stack images at 3 d.i.v. (scale bar = 100 µm, green = eGFP). **(b,c)** Analysis of **(b)** MBP$^+$ cells per FOV and **(c)** myelination index (NF200$^+$MBP$^+$) of brain stem slices with or without T_{reg} cells at 3 d.i.v., Control: MBP$^+$ counts n = 25 FOV and myelination index n = 24 FOV. T_{reg}: MBP$^+$ counts n = 15 and myelination index n = 15 FOV. Fields of view were selected from 3-6 slices/group (MBP$^+$ counts: t = 3.058, d.f. = 38, P = 0.0041; myelination index: t = 3.146, d.f. = 37, P = 0.0033, unpaired, two-tailed, Student's t test). **(d)** Representative images of brain slices from **(b, c)** taken from a z-stack image (scale bar = 100 µm, green = NF200, red = MBP). **(e)** Analysis of myelination index (NF200$^+$MBP$^+$) of brain stem slices with T_{reg} or T_{conv} cells at 3 d.i.v. T_{conv} n = 15 FOV and T_{reg} n = 14 FOV from 3-6 slices per group (U = 26, P = 0.0006, two-tailed Mann-Whitney U test). **(f)** Representative flow cytometric analysis of non-polarized (NP) T cells and T_{reg} after reactivation for 72h, FSC = Forward Scatter. **(g)** Analysis of myelination index (NF200$^+$MBP$^+$) of brain stem slices treated with non-polarized (NP) or Treg-conditioned media, at 7 d.i.v. NP n= 14 FOV and T_{reg} n = 15 FOV from 3-6 slices per group (t = 4.559, d.f. = 27, P < 0.0001, unpaired two-tailed Student's t test). **(h-j)** Electron microscopic analysis of control (non-demyelinated; M) and remyelinating (RM) brain slices with and without T_{reg}-conditioned medium, n = 3 slices/condition, scale bar = 2 µm (number of myelinated fibres: $F(2,6)$ = 22.89, P = 0.0016; g-ratio: $F(2,6)$ = 5.915, P = 0.0381, one-way ANOVA with Bonferroni *post hoc* test). Number of myelinated fibres: F = 22.89, Rsquare = 0.8841,C(M) v C(RM) t = 6.592, C(M) v Treg t = 1.978, C(RM) v Treg t = 4.614, P = 0.0016. g-ratio: F = 5.915, R square = 0.6635, C(M) v C(RM) t = 3.344, C(M) v Treg (RM) t = 2.370, p = 0.0381. **(k)** ELISA of IL-6 in brain slice culture-conditioned media up to day 6 *in vitro*. n = 4 wells, each from an independent experiment. Data shown are representative of at least 2 (**a-e, g**) 7 (**f**) or 1 (**h-j**) independent experiments. Data presented with mean values indicated, error bars = SEM, *P<0.05, ** P <0.01, *** P <0.001.

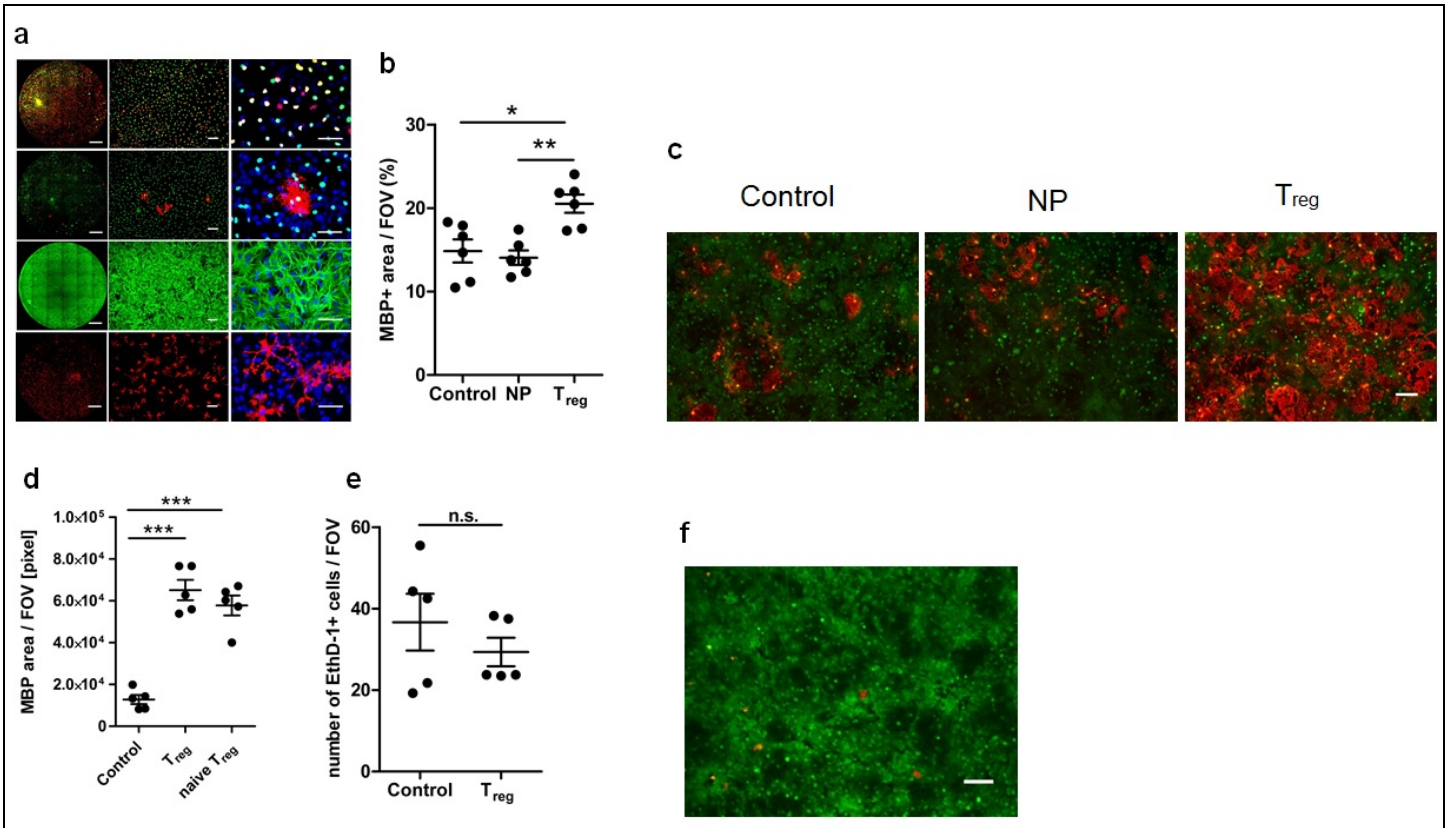

Supplementary Figure 3

T_{reg} promote oligodendrocyte differentiation in mixed glia but do not affect OPC survival in the steady state

(a) Immunofluorescence analysis of OPC (green = Olig2, red = Ki67, first row), oligodendrocyte (green = Olig2, red = MBP, second row), astrocyte (green = GFAP, third row) and microglial (red = CD11b, last row) markers after 1 week of mixed glial culture. Blue = DAPI. Left panels depict a stitched image of the well of a 96-well plate (stitched images were taken at 10x) (scale bars from left to right panels = 500 µm, 100 µm, 50 µm). **(b, c)** Immunofluorescence analysis of MBP^+ percentage area (Control vs T_{reg}: $U = 4$, $P = 0.026$; Non-Polarized (NP) vs T_{reg}: $U = 1$, $P = 0.0043$, two-tailed Mann-Whitney U test) and **(c)** representative images of mixed glial cultures after 5 days of indicated treatment, n=6, (scale bar = 100 µm, green = Olig2, red = MBP). **(d)** Immunofluorescence analysis of MBP^+ area of mixed glial cultures after 5 days in the presence of T_{reg}-conditioned media prepared from total, or naïve, $CD4^+$ T cells, n = 5 (Control vs T_{reg}: $t = 9.786$, d.f. = 8, $P < 0.0001$; control vs naïve T_{reg}: $t = 8.644$, d.f. = 8, $P < 0.0001$; T_{reg} vs naïve T_{reg}: $t = 1.079$, d.f. = 8, $P = 0.3119$, unpaired two-tailed Student's t test). **(e,f)** Immunofluorescence analysis of EthD-1^+ cell numbers, n = 5, ($U = 10$, $P = 0.6752$, Mann Whitney U test) and **(f)** representative images of mixed glial cultures (scale bar = 100 µm, green = calcein, red = EthD-1). Data representative of **(b)** 3 and **(d,e)** 2 independent experiments. Data presented with mean values indicated, error bars = SEM, * $P<0.05$, ** $P<0.01$.

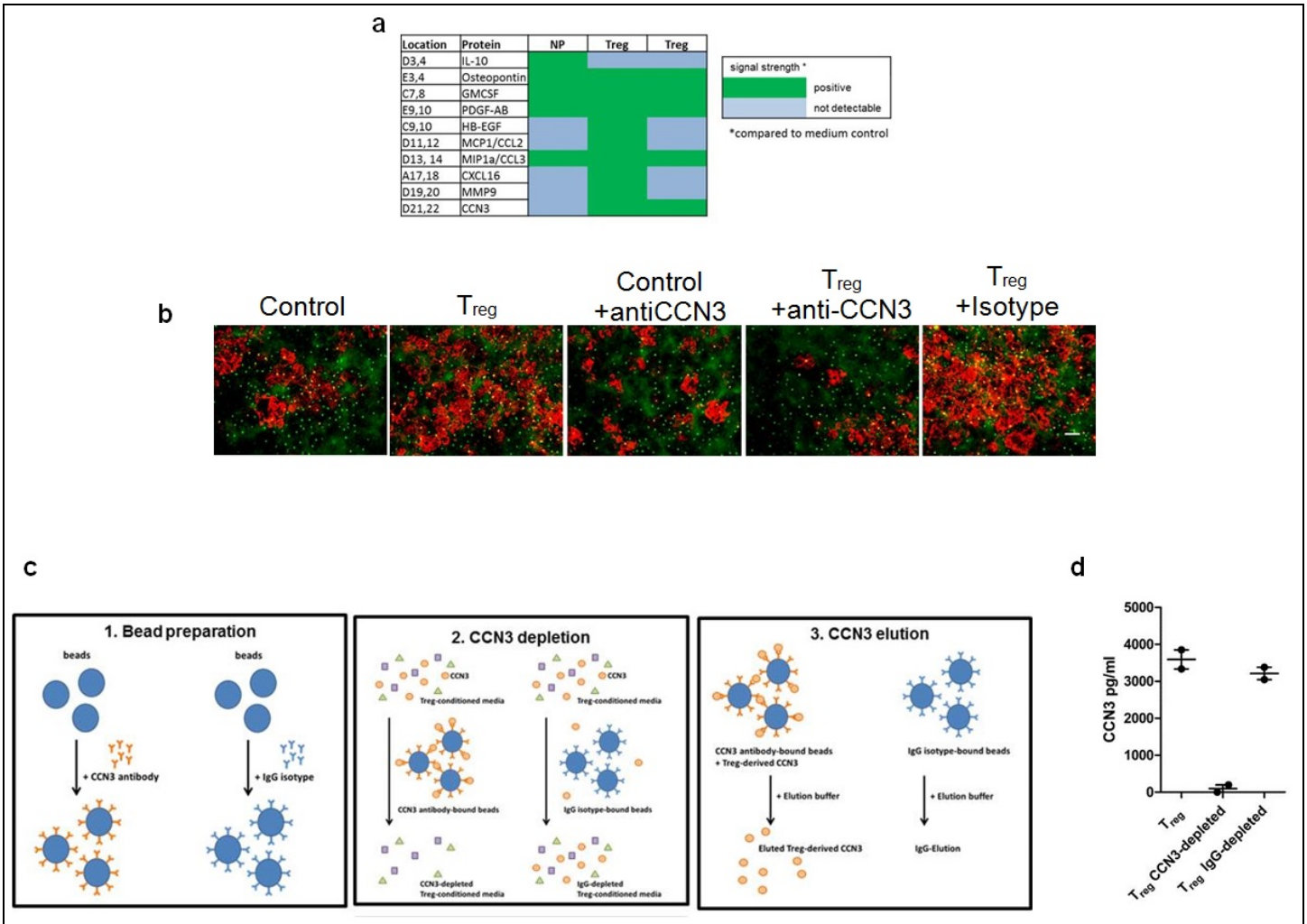

Supplementary Figure 4

Identification of CCN3 as a mediator of T_{reg}-induced oligodendrocyte differentiation

(a) Semi-quantitative proteome profiler analysis of non-polarized (NP) and T_{reg}-conditioned media (2 independent batches) compared to cell culture medium only. **(b)** Representative immunofluorescence images of mixed glial cultures stained for $Olig2^{+}MBP^{+}$ cells and analyzed quantitatively in **(Figure 4d)** (Green = Olig2, red = MBP, scale bar = 100 µm). **(c)** Schematic diagram of CCN3 depletion and elution from T_{reg}-conditioned media. **(d)** ELISA confirmation of CCN3 depletion from T_{reg}-conditioned media n = 2. Data representative of 1 **(a,** with 2 independently generated batches**)**, or at least 3 **(b, d)** biologically independent experiments.